7-2014

Radar Image Processing and Its Applications Based on Convolution Back Projection

Qitong Li
University of Texas-Pan American

RADAR IMAGE PROCESSING AND ITS APPLICATIONS BASED ON CONVOLUTION BACK PROJECTION

A Thesis

by

QITONG LI

Submitted to the Graduate School of the
University of Texas-Pan American
In partial fulfillment of the requirements for the
degree of

MASTER OF SCIENCE

July 2014

Major Subject: Mathematical Sciences

RADAR IMAGE PROCESSING AND ITS APPLICATIONS BASED ON CONVOLUTION BACK PROJECTION

A Thesis
by
QITONG LI

COMMITTEE MEMBERS

Dr. Zhijun Qiao
Chair of Committee

Dr. Paul Bracken
Committee Member

Dr. Timothy Huber
Committee Member

Dr. Karen Yagdjian
Committee Member

July 2014

ABSTRACT

Li, Qitong, Radar Image Processing and its applications based on Convolution Back Projection. Master of Science (MS), July, 2014, 38 pages, 17 figures, 16 references,18 titles.

A general synthetic aperture radar (SAR) signal model is derived from the Maxwell's equations, and a SAR image processing algorithm called Convolution Back Projection (CBP) will be introduced in this thesis, which can be applied to data gathered by a Synthetic Aperture Radar (SAR) system to produce high resolution images. The purpose of this thesis is starting from Maxwell's equations to study the CBP algorithm as it is applied to SAR image processing. Two different image simulation results will be provided by this method.

DEDICATION

I would like to dedicate this thesis to my family for their unconditional love and support. Thank you for all your love and support, with your love, I can conquer anything.

ACKNOWLEDGMENTS

I am grateful to my advisor Dr. Zhijun Qiao, for his guidance and patience while helping me formulate this work. I would also like to express my sincere thanks to other students in Dr. Qiao's research group.

TABLE OF CONTENTS

LIST OF FIGURES

CHAPTER I

INTRODUCTION

Radar is an acronym that stands for Radio Detection and Ranging. It is a remote sensing technology that uses electromagnetic radiation in the radio or microwave spectrum to detect objects over large distances. From its name, it should be clear that a true radar system must be able to both detect a target and determine its distance from the radar antenna. However, modern systems have a number of other added capabilities. For example, some radar systems are able to measure the velocity of a target in terms of the doppler-shift induced by the motion of the target, which may be either linear or rotational. Another very important application of radar is the production of high resolution images.

It is the application of radar technology to the image formation problem that will be the subject of this this thesis. Specifically the application of convolution backprojection (CBP) to the problem of radar imaging will be considered. The most common radar imaging technology that is currently in use is synthetic aperture radar (SAR), which uses the motion of the radar antenna with respect to a stationary target to improve image resolution when compared to a stationary antenna. These techniques discussed in this thesis can also easily be applied to a similar imaging problem where the target is moving and the antenna is stationary. This method is referred to as inverse synthetic aperture radar (ISAR).

The CBP is algorithm is a computerized tomographic imaging technique that was originally developed for medical imaging applications. This imaging method has since been expanded to a variety of different fields. These include radio astronomy, geophysics, and sonar. The application of the CBP to radar is a relatively new development, dating to the middle of the1980s. Prior to the introduction of backprojection algorithms, the primary method used in radar image reconstruction were direct Fourier techniques such as the polar format algorithm.

The purpose of this thesis is to study the CBP algorithm as it is applied to SAR image formation. This algorithm will be formulated based on a common radar wave model, which can be derived from Maxwell's Equations. In specific, a formulation of the CBP algorithm for the case of a circular SAR system will be presented. The key to development that will be used to formulate the CBP algorithm is the projection-slice theorem.

CHAPTER II

SYNTHETIC APERTURE RADAR

II.1 Synthetic Aperture Radar (SAR)

Synthetic aperture radar (SAR) is a remote sensing technique that uses an antenna, which is mounted on a moving platform, to image a stationary target scene. In most cases, SAR antennas are either mounted on airborne or spaceborne platforms, such as airplanes or satellites. These antennas use highly directed microwave radiation to produce images of specific patch of the Earth's surface. Unlike most remote imaging systems such as visible and infrared systems, SAR uses active imaging [5, 8]. This means that the portion of the ground that is to be imaged must first be illuminated by a beam of microwave energy emitted by a transmitting antenna, rather than relying on passive sources of illumination such as solar radiation. SAR systems are also preferred over other types due to their ability to produce high quality images through cloud cover and at night [4].

In the early 1950's, Carl Wiley discovered a novel method to increase the cross-range resolution of radar imaging systems, which he referred as a Doppler beam sharpening [5]. What he discovered was that a comparison of the returns from a series of radar pulses from an antenna mounted on a platform moving along a given flight path parallel to the ground could be used to produce a higher resolution image [2]. In this way, a synthetic aperture with length equal to that of the platform flight path is created. The method that he discovered was essentially the same as what is now called stripmap-mode SAR.

II.2 Two modes of SAR Imaging

There are a number of different types of SAR imaging systems that are currently in use. Two of the most common SAR modes, which are used by modern systems, are stripmap-mode and spotlight-mode. However, it should be noted that these modes are not exclusive. That is, there are some SAR systems that can switch between imaging modes [4].

As was previously mentioned, the original SAR mode that was invented byWiley was stripmap-mode SAR. In the case of this SAR mode, the radar antenna is mounted at a fixed angle on a moving platform. stripmap-mode SAR systems are capable of producing high resolution images over a large region of the ground. This makes it useful for terrain mapping.

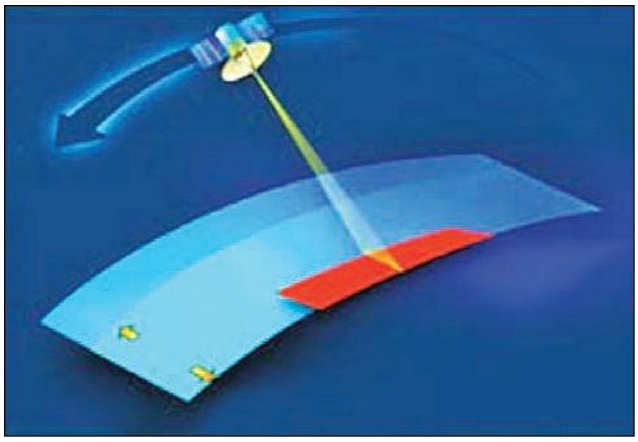

Figure II.1: Illustration of stripmap-mode SAR

The conventional SAR stripmap-mode assumes a fixed pointing direction of the radar antenna broadside to the platform track. A strip map is an image formed in width by the swath of the SAR and follows the length contour of the flight line of the platform itself.

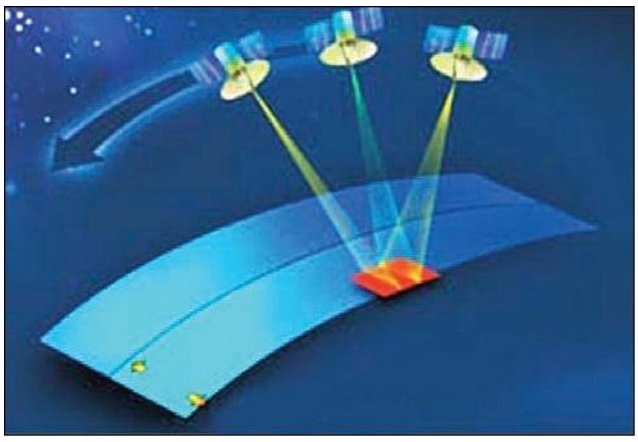

Figure II.2: Illustration of spotlight-mode SAR

Spotlight-SAR is a mode of SAR operation for obtaining high resolution by steering the radar beam to keep the target within the beam for a longer time and thus form a longer synthetic aperture. Spotlight SAR is capable of extending the high-resolution SAR imaging capability significantly.

As more pulses are used, the azimuth resolution increases. This is achieved by keeping a target within the spotlight illumination of the radar beam for a longer time through electronic beam steering, resulting in a longer synthetic aperture. Spotlight SAR mode of operation is usually at the expense of spatial coverage, as other areas within a given accessibility swath of the SAR cannot be illuminated while the radar beam is spotlighting over a particular target area.

CHAPTER III

MATHEMATICAL MODEL FOR SAR

III.1 Maxwell's Equations

A mathematical model for the propagation of radar signals in free space will be derived in this section.The proper model for electromagnetic waves propagation is based on Maxwell's equations, and they are listed below

$$\boldsymbol{\nabla} \times \mathbf{E} = -\partial_t \mathbf{B}, \tag{III.1a}$$

$$\boldsymbol{\nabla} \times \mathbf{H} = \mathbf{J} + \partial_t \mathbf{D}, \tag{III.1b}$$

$$\boldsymbol{\nabla} \cdot \mathbf{E} = \rho, \tag{III.1c}$$

$$\boldsymbol{\nabla} \cdot \mathbf{B} = 0. \tag{III.1d}$$

The quantities given in the above equations are:

- $\mathbf{D}(t, \mathbf{x})$ - electric displacement field
- $\mathbf{E}(t, \mathbf{x})$ - electric field
- $\mathbf{B}(t, \mathbf{x})$ - magnetic induction field
- $\mathbf{H}(t, \mathbf{x})$ - magnetic field
- $\mathbf{J}(t, \mathbf{x})$ - current density
- $\rho(t, \mathbf{x})$ - charge density

The electric displacement field and the electric field, and the magnetic induction field and the magnetic field are related by

$$\mathbf{B} = \mu\mathbf{H} \qquad \text{and} \qquad \mathbf{D} = \epsilon\mathbf{E}.$$

where,

- $\mu(\mathbf{x}, t)$ is the permeability of the medium of propagation.
- $\epsilon(\mathbf{x}, t)$ is permittivity of the medium propagation.

We assume that $\mathbf{x} = \mathbf{x}_0$, $\mathbf{x}_0 \in \mathbb{R}^3$ is antenna location, current density $\mathbf{J}(t, \mathbf{x}) \neq \mathbf{0}$. Otherwise, $\mathbf{J}(t, \mathbf{x}) = \mathbf{0}$. In addition, $\rho(t, \mathbf{x}) = 0$ for all $\mathbf{x} \in \mathbb{R}^3$. Then the following equations can be derived from Maxwell's equations

$$\boldsymbol{\nabla} \times \mathbf{E} = -\partial_t \mathbf{B}, \tag{III.2a}$$

$$\boldsymbol{\nabla} \times \mathbf{B} = \mu_0 \mathbf{J} + \mu_0 \epsilon_0 \partial_t \mathbf{E}, \tag{III.2b}$$

$$\boldsymbol{\nabla} \cdot \mathbf{E} = 0. \tag{III.2c}$$

Applying the curl operator to both sides of (III.2a). Then, the left hand side is given by the well know identity

$$\boldsymbol{\nabla} \times \boldsymbol{\nabla} \times \mathbf{E} = \boldsymbol{\nabla}(\boldsymbol{\nabla} \cdot \mathbf{E}) - \boldsymbol{\nabla}^2 \mathbf{E}.$$

After applying (III.2b) the following wave equation is derived

$$\left(\boldsymbol{\nabla}^2 - \mu_0 \epsilon_0 \partial_t^2 \right) \mathbf{E}(t, \mathbf{x}) + \mu_0 \partial_t \mathbf{J}(t, \mathbf{x}) = 0. \tag{III.3}$$

Substitute the identity $\mu_o \epsilon_0 = c_0^{-2}$ yielding that equation (III.3) is

$$\left(\boldsymbol{\nabla}^2 - \frac{1}{c_0^2}\partial_t^2\right)\mathbf{E}(t,\mathbf{x}) + \mu_0\partial_t\mathbf{J}(t,\mathbf{x}) = 0. \tag{III.4}$$

Similarly, we can get the following equation as well,

$$\left(\boldsymbol{\nabla}^2 - \frac{1}{c_0^2}\partial_t^2\right)\mathbf{H}(t,\mathbf{x}) + \nabla \times \mathbf{J}(t,\mathbf{x})t = 0. \tag{III.5}$$

In many cases, these two wave equations can be used to model radar waves in place of Maxwell's equations. But it is customary to use the electric field.

III.2 Scalar Wave Propagation

In the previous section, it was determined that the radar waves can be modeled by the nonhomogeneous scalar wave equation (III.3). In general, the following wave equation can be used in the place of (III.4).

$$\left(\nabla^2 - \frac{1}{c^2(\mathbf{x})}\partial_t^2\right)u(t,\mathbf{x}) = -j(t,\mathbf{x}). \tag{III.6}$$

Where, $u = E_i$ for $1 \leq i \leq 3$ represents one component of the electromagnetic field due to some source $j = \mu_0\partial_t J_i$. And $c(x)$ is local propagation speed of electromagnetic waves.

In this model, the electric field can be divided into two component fields

$$u = u^{\text{in}} + u^{\text{sc}}.$$

In the above equation, $u^{\text{in}}(t,\mathbf{x})$ is the incident field that is emitted by the antennas, and u^{sc} is the scattered field, which results from the interaction of the incident field with a target. Since the source of the incident field is a current on the antenna, u^{in} is modeled using the following wave equation.

$$\left(\nabla^2 - \frac{1}{c_0^2}\partial_t^2\right)u^{\text{in}}(t,\mathbf{x}) = -j(t,\mathbf{x}), \tag{III.7}$$

A wave equation that describes the propagation of the scattered field is derived from (III.6) and

(III.7). This equation is given as follows

$$\left(\nabla^2 - \frac{1}{c_0^2}\partial_t^2\right) u^{sc}(t,\mathbf{x}) = -V(\mathbf{x})\partial_t^2 u(\mathbf{x},t). \tag{III.8}$$

Where $V(\mathbf{x})$ is a reflectivity function, which is given by:

$$V(\mathbf{x}) = \frac{1}{c_0^2} - \frac{1}{c^2(\mathbf{x})}.$$

When the incident field comes into contact with a target, it induces a current, which causes the target to re-emit a weaker time shifted version of the same signal. However, $V(\mathbf{x})$ does not directly measure the intensity of the reflected signal. Instead, it indicates the level perturbation that occurs in the wave speed when the incident field comes in contact with the target plane. It will be assumed that the reflectivity function has compact support on the set of points on the target plane that have been illuminated by the antenna. A fundamental solution of the wave equation is a generalized function satisfying

$$\left(\nabla^2 - \frac{1}{c_0^2}\partial_t^2\right) g^{\text{in}}(t,\mathbf{x}) = -\delta(t)\delta(\mathbf{x}),$$

And the solution to this equation is [3, 7]

$$g(t,\mathbf{x}) = \frac{\delta(t - |\mathbf{x}|/c_0)}{4\pi|\mathbf{x}|}.$$

The Green's function enables us to solve the constant-speed wave equation with any source term. Then, the solution for the incident field is

$$u^{\text{in}}(t,\mathbf{x}) = \int_{\mathbb{R}^3} d\mathbf{y} \int_{\mathbb{R}} d\tau \frac{\delta(t - \tau - |\mathbf{x}-\mathbf{y}|/c_0)}{4\pi|\mathbf{x}-\mathbf{y}|} j(\tau,\mathbf{y}). \tag{III.9}$$

In the case of this model, the incident field u^{in} will be produced by a single stationary isotropic point antenna $\mathbf{x}_0 \in \mathbb{R}^3$. Given this assumption, a time varying signal given by p can be introduced. Since the antenna current density will be modeled such that $j(t,\mathbf{x}) = p(t)\delta(\mathbf{x} - \mathbf{x}_0)$. Subsisting

this into III.9 yields

$$u^{\text{in}}(t, \mathbf{x}) = \frac{p(t - |\mathbf{x} - \mathbf{x_0}|/c_0)}{4\pi|\mathbf{x} - \mathbf{x_0}|}. \tag{III.10}$$

Furthermore, it is common to represent the current wave model in the frequency domain. Such a representation can be found by considering the following Helmholtz wave equation

$$\left(\nabla^2 + k^2\right) u^{\text{in}}(t, \mathbf{x}) = -J(\mathbf{x}, f). \tag{III.11}$$

In the above equation, u^{in} and $J(\mathbf{x}, f)$ are the Fourier transforms of u^{in} and $j(\mathbf{x}, f)$, respectively. This equation can be solved using the Helmholtz Green's function

$$G_f(\mathbf{x}) = \frac{e^{-ik|\mathbf{x}|}}{4\pi|\mathbf{x}|}.$$

Note, in the above equation $k = \dfrac{2\pi f}{c_0}$ denotes the wavenumber. Then, the solution for the frequency domain representation of the incident field is given in terms of the following equation

$$U^{\text{in}}(\mathbf{x}, f) = \int_{R^3} \frac{e^{-ik|\mathbf{x}-\mathbf{y}|}}{4\pi|\mathbf{x} - \mathbf{y}|} J(\mathbf{x}, f)\, d\mathbf{y} \tag{III.12}$$

since $j(t, \mathbf{x}) = p(t)\delta(\mathbf{x} - x_0)$, we obtain

$$U^{\text{in}}(\mathbf{x}, f) = P(f)\frac{e^{-ik|\mathbf{x}-\mathbf{x}_0|}}{4\pi|\mathbf{x} - \mathbf{x}_0|}, \tag{III.13}$$

where $U^{\text{in}}(\mathbf{x}, f)$ is the Fourier transform of $u(t, \mathbf{x})$.

III.3 The Lippman-Schwinger Integral Equation

Since the scattered field is created as a result of the interaction of the incident field with the target scene, it would be useful if a formulation for the scattered field could be found directly in terms of the incident field. However, in general, this is not always possible. Consider that the

scattered field can be described by the following equation

$$\left(\nabla^2 + k^2\right) U^{sc}(\mathbf{x}, f) = V(\mathbf{x})U(\mathbf{x}, f). \tag{III.14}$$

The solution to this equation can be found, in the same way as before, in the frequency domain to be

$$U^{\text{sc}}(\mathbf{x}, f) = -(2\pi f)^2 \int_{\mathbb{R}^3} \frac{e^{-ik|\mathbf{x}-z|}}{4\pi|\mathbf{x}-\mathbf{z}|} V(\mathbf{z})U(\mathbf{z}, f)\, d\mathbf{z}, \tag{III.15}$$

and in the time domain to be

$$u^{\text{sc}}(\mathbf{x}, f) = \int_{\mathbb{R}^3} d\mathbf{z} \int_{\mathbb{R}} d\tau \frac{\delta(t-\tau-|\mathbf{x}-\mathbf{z}|/c_0)}{4\pi|\mathbf{x}-\mathbf{z}|} V(\mathbf{x})\partial_t^2 u(\mathbf{z}, t). \tag{III.16}$$

It is clear that in both of the above expressions that the scattered field is dependent on the total field. Since in the last two equations the scattered field appears on both sides of the equation, it is not possible to exactly formulate the scattered field in terms of the incident field alone. In the following two sections, a solution to this problem will be detailed.

III.4 The Born Approximation

For radar imaging, we measure u^{sc} at the antenna, and we would like to determine V. However, bothe V and u^{sc} in the neighborhood of the target V are unknown, and in III.16 these unknowns are multiplied together. This nonlinearity makes it difficult to solve for V . Consequently, almost all work on radar imaging involves making the Born approximation, which is also known as the weak-scattering or single-scattering approximation. This corresponds to replacing u^{sc} on the right side of III.16 by u^{in} giving the following equation

$$\begin{aligned} u^{\text{sc}}(\mathbf{x}, t) &= \int_{\mathbb{R}^3} d\mathbf{z} \int_{\mathbb{R}} d\tau \frac{\delta(t-\tau-(|\mathbf{z}-\mathbf{x}_0|+|\mathbf{x}-\mathbf{z}|)/c_0)}{(4\pi)^2|\mathbf{z}-\mathbf{x}_0||\mathbf{x}-\mathbf{z}|} V(\mathbf{z})\partial_t^2 u^{\text{in}}(\mathbf{z}, t) \\ &= \int_{\mathbb{R}^3} \frac{\ddot{p}_n(t-(|\mathbf{z}-\mathbf{x}_0|+|\mathbf{x}-\mathbf{z}|)/c_0)}{(4\pi)^2|\mathbf{z}-\mathbf{x}_0||\mathbf{x}-\mathbf{z}|} V(\mathbf{z})\, d\mathbf{z}. \end{aligned} \tag{III.17}$$

And in frequent domain, the born approximation is

$$\begin{aligned} U^{\text{sc}}(\mathbf{x}, f) &= -(2\pi f)^2 \int_{\mathbb{R}^3} \frac{e^{-ik|\mathbf{x}-z|}}{4\pi|\mathbf{x}-\mathbf{z}|} V(\mathbf{z}) U^{\text{in}}(\mathbf{z}, f)\, d\mathbf{z} \\ &= -(2\pi f)^2 P(f) \int_{\mathbb{R}^3} \frac{e^{-ik|\mathbf{z}-\mathbf{x}_0|} e^{-ik|\mathbf{x}-\mathbf{z}|}}{(4\pi)^2 |\mathbf{z}-\mathbf{x}_0||\mathbf{x}-\mathbf{z}|} V(\mathbf{z})\, d\mathbf{z}. \end{aligned} \tag{III.18}$$

With this linearized approximation for the scattered field, it is now possible to model the signal that is returned to each receiving antenna.

III.5 Recieved Signal

For the received signal, which is given by $s(t)$, can be found by evaluating the scattered field at the antenna position $\mathbf{x}_0$. In this case, the equation for the received signal is given by:

$$S(f) = U^{\text{sc}}(\mathbf{x}_0, f) = -(2\pi f)^2 P(f) \int_{\mathbb{R}^3} \frac{e^{-i2k|\mathbf{z}-\mathbf{x}_0|}}{(4\pi)^2 (|\mathbf{z}-\mathbf{x}_0|)^2} V(\mathbf{z}) d\mathbf{z}. \tag{III.19}$$

Also, the time varying version of the scattered field is given by:

$$s(t) = \int_{\mathbb{R}^3} \frac{\ddot{p}(t - 2|\mathbf{z}-\mathbf{x}_0|/c_0)}{(4\pi)^2 |\mathbf{z}-\mathbf{x}_0|^2} V(\mathbf{z}) d\mathbf{z}. \tag{III.20}$$

The computation of the incident field can be simplified by eliminating the second derivative in equation III.19. This can be accomplished by choosing the baseband signal $a(t)$, such that it is slowly varying in relation to the carrier signal. Given this assumption the second derivative of the incident field can be approximated by $\ddot{p}(t) \approx -4\pi^2 f_c^2 p(t)$. For a linear chirp signal of the form given in section II.4, it would be beneficial to find a criteria for K and T such that this condition holds. This can be done by first writing the chirp signal in equation II.5 as $p_{\text{chirp}}(t) = e^{iq(t)}$, where $q(t) = Kt^2 + 2\pi f_c t$. Next, taking the second derivative shows that

$$\ddot{p}_{\text{chirp}}(t) = \partial_t^2 e^{iq(t)} = \left\{ i\ddot{q}(t) - (\dot{q}(t))^2 \right\} e^{iq(t)}. \tag{III.21}$$

Then, computing the bracketed terms gives:

$$i\ddot{q}(t) - (\dot{q}(t))^2 = 4\pi^2 f_c^2 \left\{ -\left(1 + \frac{Kt}{2\pi f_c}\right)^2 + \frac{iK}{4\pi^2 f_c^2} \right\}. \tag{III.22}$$

From the computation above, it can be concluded that

$$\ddot{p}_{\text{chirp}}(t) \approx -4\pi^2 f^2 p_{\text{chirp}}(t),$$

when

$$\frac{K}{4\pi^2} << f_c^2 \qquad \text{and} \qquad \frac{Kt}{2\pi} << f_c.$$

Under this condition the second derivative can be omitted from III.20, and the factor $-(2\pi f)^2$ can be dropped in III.19. Thus, the expressions for the scattered field is

$$S(f) = U^{\text{sc}}(\mathbf{x}_0, f) = P(f) \int_{\mathbb{R}^3} \frac{e^{-i2k|\mathbf{z}-\mathbf{x}_0|}}{(4\pi)^2(|\mathbf{z}-\mathbf{x}_0|)^2} V(\mathbf{z}) d\mathbf{z}, \tag{III.23}$$

$$s(t) = \int_{\mathbb{R}^3} \frac{p(t - 2|\mathbf{z}-\mathbf{x}_0|/c_0)}{(4\pi)^2|\mathbf{z}-\mathbf{x}_0|^2} V(\mathbf{z}) d\mathbf{z}. \tag{III.24}$$

This model can be applied for any monostatic radar system. A model that is more specific to SAR can be found by replacing $\mathbf{x}_0$ with a time varying function $\mathbf{\Gamma}(t)$, which represents the motion of the antenna along its flight path. The range from the antenna to the target can now be characterized in terms of the function $R(\mathbf{z}, t) = |\mathbf{z} - \mathbf{\Gamma}(t)|$. The equation for the received signal can now be written as

$$S(f) = P(f) \int_{\mathbb{R}^3} \frac{e^{-i2kR(\mathbf{z},t)}}{(4\pi)^2 R^2(\mathbf{z}, t)} V(\mathbf{z}) d\mathbf{z}. \tag{III.25}$$

III.6 Circular SAR modle

It was mentioned that the CBP algorithm is well suited to spotlight-mode SAR image formation. However, spotlight-mode SAR was developed based on early experiments with targets on a rotating turntable [13, 18, 10]. This is referred to as turntable-ISAR. Turntable-ISAR is mathemat-

ically equivalent to the case of an antenna moving in a circular path around a fixed target. It is this case that will be considered in this section.

For the sake of mathematical simplicity, it will be assumed that the all targets lie on a flat ground topography. Hence, all will be located within a bounded subset Ω of the x_1, x_2-plane. As pictured in Figure III.1, the antenna will move counter-clockwise along a circular path of radius r, with its center right above the origin. This flightpath will remain parallel to the ground plane with fixed height h. It will also be assumed, that the starting point of the radar platform will be located over the x_1-axis.

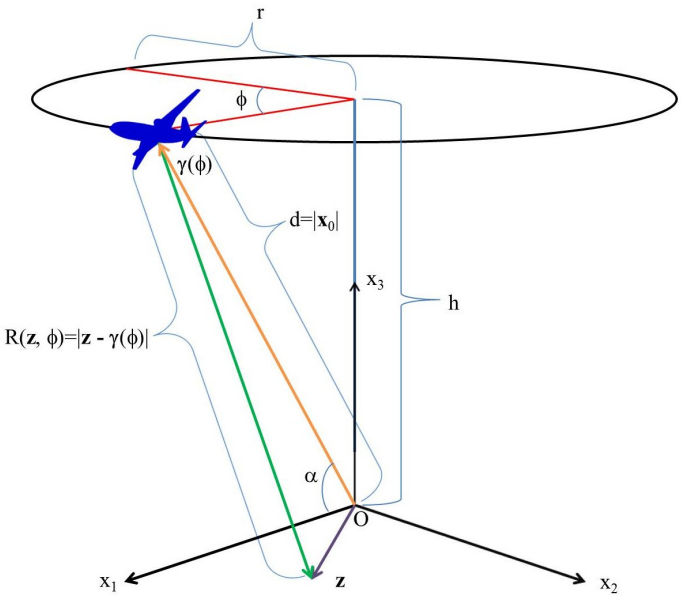

Figure III.1: Circular SAR Geometry

The range from a point $\mathbf{z} \in \Omega$ was found to be $R(\mathbf{z}, t) = |\mathbf{z} - \mathbf{\Gamma}(t)|$, where $\mathbf{\Gamma}(t)$ indicates the time dependent position along the antenna path. For the flight path described by Figure III.1, the antenna path is defined by

$$\mathbf{\Gamma}(t) = (r\cos(\omega t), r\sin(\omega t), h)^T.$$

This definition is appropriate, since the distance $d = \sqrt{r^2 + h^2}$, from the origin to the antenna remains fixed as the antenna moves along the circular path. This implies that only the angular displacement varies with respect to time. The angular displacement of the antenna is denoted by

$\phi(t) = \omega t$.

In this case, the system used is a pulsed radar system. That is to say, the radar antenna will emit a series of short duration microwave pulses as it moves along its flight path. Letting t_{n_1}, t_{n_2} be the initial and final times, respectively, for the n^{th} pulse, the antenna will move from $\phi(t_{n_1})$ to $\phi(t_{n_2})$. The angular velocity ω should be small enough, in comparison to the wave speed c_0, such that the difference between $\phi(t_{n_1})$ and $\phi(t_{n_2})$ is miniscule. In this case, a single angular displacement value $\phi(t_n)$ can be used for each pulse. This is equivalent to the Start-Stop approximation that is commonly used in radar applications [3]. Then, the flight path can be represented by a function that only depends on the angle ϕ, and which is given by

$$\boldsymbol{\gamma}(\phi) = (r\widehat{\boldsymbol{\mu}}(\phi), h)^T,$$

where

$$\widehat{\boldsymbol{\mu}} \in S^1$$

. Note that S^1 is the unit sphere in $\mathbb{R}^2$ and $\widehat{\boldsymbol{\mu}}(\phi) = (\cos\phi, \sin\phi)^T$.Then, the range from the antenna to a point $\mathbf{z} \in \Omega$ can be defined, in terms of $\boldsymbol{\gamma}(\phi)$, as

$$R(\mathbf{z}, \phi) = |\mathbf{z} - \boldsymbol{\gamma}(\phi)|.$$

Often the flight path of the radar platform is designed in such a way that the maximum target distance from the origin, which is located at the target scene center, is much smaller than the distance of the antenna from the same origin. In this case, any computation of the received signal based on equation III.20 can be simplified through the application of what is commonly referred to as the far-field approximation. This approximation can be understood by first noting that radar waves propagate as a spherical wave front. When the antenna is far from the target center, the curvature of this wavefront can be assumed to be negligible. Under this assumption, in the extreme far-field, radar wave propagation can be approximately represented by a plane wave. This assump-

tion can be justified mathematically by applying a first order Taylor expansion to the range term $|\mathbf{z} - x_0|$

$$|\mathbf{z} - \mathbf{x}_0| = \sqrt{|\mathbf{z}|^2 + |\mathbf{x}_0|^2 - 2\mathbf{z}\cdot\mathbf{x}_0} = |\mathbf{x}_0| - \widehat{\mathbf{x}}_0 \cdot \mathbf{z} + O\left(\frac{|\mathbf{z}|^2}{|\mathbf{x}_0|}\right).$$

Then, the phase term becomes

$$e^{-ik|\mathbf{z}-\mathbf{x}_0|} = e^{-i2k|\mathbf{x}_0|} e^{i2\widehat{\mathbf{x}}_0\cdot\mathbf{z}} \left(1 + O\left(\frac{k|\mathbf{z}|^2}{|\mathbf{x}_0|}\right)\right).$$

Similarly, the Taylor expansion can be applied to the geometric spreading factor $|\mathbf{z} - \mathbf{x}_0|^{-2}$ from the denominator of III.20 such that

$$|\mathbf{z} - \mathbf{x}_0|^{-2} = \frac{1}{|\mathbf{z}|^2 + |\mathbf{x}_0|^2 - 2\mathbf{z}\cdot\mathbf{x}_0} = \frac{1}{|\mathbf{x}_0|^2}\left(1 + O\left(\frac{|\mathbf{z}|^2}{|\mathbf{x}_0|^2}\right)\right).$$

This shows that when $|\mathbf{y}| << |\mathbf{x}_0|$ and $k|\mathbf{z}|^2 << |\mathbf{x}_0|$[1], the recieved signal can be approximately written as follows.

$$\begin{aligned} S(f,\phi) &\approx \frac{e^{-i2k|\boldsymbol{\gamma}(\phi)|}}{(4\pi)^2|\boldsymbol{\gamma}(\phi)|^2} P(f) \int_{\mathbb{R}^3} V(\mathbf{z}) e^{i2k\widehat{\boldsymbol{\gamma}(\phi)}\cdot\mathbf{z}} d\mathbf{z} \\ &= \frac{e^{-i2k|\boldsymbol{\gamma}(\phi)|}}{(4\pi)^2|\boldsymbol{\gamma}(\phi)|^2} P(f) \mathscr{F}_{\mathbb{R}^3}\{V\}(-2k\widehat{\boldsymbol{\gamma}(\phi)}). \end{aligned} \tag{III.26}$$

The reflectivity function V could be recovered by moving all of the factors in front of the Fourier transform to the other side of equation (III.23), and then applying the inverse Fourier transform to the result

$$V(\mathbf{z}) = (4\pi)^2 \mathscr{F}^{-1}_{\mathbb{R}^3}\left\{\frac{|\boldsymbol{\gamma}(\phi)|^2 e^{i2k|\boldsymbol{\gamma}(\phi)|} S(f,\phi)}{P(f)}\right\}. \tag{III.27}$$

This method of recovering the reflectivity values is commonly referred to as source deconvolution [11, 12]. In actual applications this method is impractical, since $P(f)$ is band-limited. This means that $P(f)$ is zero outside of a neighborhood with radius equal to the bandwidth. The implementation of this procedure could lead to a division by zero. However, there are several methods that

are commonly used to approximate this method. For example, one common method that is often used is called deramp processing [5, 9]. This method involves multiplying the received signal by the complex quadrature form of the transmitted signal, applying a low pass filter to this product, and then taking the Fourier transform of the result. This particular method is often used to process data from Spotlight-mode SAR systems.

Deramp processing is an example of a common method, which is referred to as pulse compression[4]. The primary purpose of pulse compression is to maximize the SNR while maintaining high range resolution. Another common method of pulse compression is implemented by multiplying the received signal by the complex conjugate of the transmitted signal $\overline{P(f)}$. In order to understand why this substitution is made, consider that, on the interval $[f_c - \frac{f_b}{2}, f_c + \frac{f_b}{2}]$,

$$\frac{1}{P(f)} = \frac{\overline{P(f)}}{|P(f)|^2}$$

Given a linear chirp signal of form in [3]

$$\begin{aligned} p(t) &= \text{rect}\left(\frac{t}{T}\right) e^{i\pi K t^2} e^{i2\pi f_c t} \\ &= \text{rect}\left(\frac{t}{T}\right) e^{i\Phi(t)}, \end{aligned} \tag{III.28}$$

where

$$\text{rect}(t) = \begin{cases} 1 & -\frac{1}{2} \leq t \leq \frac{1}{2} \\ 0 & \text{otherwise} \end{cases},$$

pulse compression can be implemented by multiplying the received signal by the complex conjugate of the transmitted signal $\overline{P(f)}$. The result will then be multiplied by $(4\pi)^2|\boldsymbol{\gamma}(\phi)|$. This compensates for the power loss due to the geometric spreading that occurs as a wave moves away from its source. Also, in order to compensate for the phase offset due to the range, the pulse compressed signal should also be multiplied by the factor $e^{i2k|\boldsymbol{\gamma}(\phi)|}$. The result of these operations will

be the following data function

$$\begin{aligned} D(f,\phi) &= (4\pi)^2|\boldsymbol{\gamma}(\phi)|^2 e^{i2k|\boldsymbol{\gamma}(\phi)|}\overline{P(f)S(f,\phi)} \\ &= |P(f)|^2 \int_{\mathbb{R}^3} V(\mathbf{z}) e^{i2k\widehat{\boldsymbol{\gamma}(\phi)}\cdot\mathbf{z}} d\mathbf{z} \\ &= |P(f)|^2 \mathscr{F}_{\mathbb{R}^3}\{V\}(-2k\widehat{\boldsymbol{\gamma}(\phi)}). \end{aligned} \tag{III.29}$$

The data function is composed of a set of range profiles for every fixed value of ϕ. This will be illustrated.

Pulse compression is equivalent to the time domain operation known as matched filtering. A matched filter is implemented by applying the correlation of the time domain received signal with the complex conjugate of the incident wave $\overline{p(t)}$. This operation is characterized by

$$\eta_\phi(t) = \int_{\mathbb{R}} \overline{p(t')} s(\widetilde{t} - t', \phi) dt', \tag{III.30}$$

where

$$\widetilde{t} = t - 2|\boldsymbol{\gamma}(\phi)|/c_0,$$

and

$$\eta_\phi(t) = \frac{d(t - 2|\boldsymbol{\gamma}(\phi)|/c_0, \phi)}{(4\pi)^2|\boldsymbol{\gamma}(\phi)|^2}.$$

The main reason that the matched filter is often used in radar imaging applications is because it has been shown to optimize the SNR [3, 5].

The data collection region is determined by $2k\widehat{\boldsymbol{\gamma}(\phi)}$. Hence, the shape of the data collection annulus will depend on the flight path geometry and the radar bandwith.

The function described by equation (III.29) represents a set of radar data, which is collected in a finite region of three dimensional wavenumber domain. As is shown in Figure III.2, the data collection region for a Circular SAR system described in Section IV.1 will be given by an annular region. This region is determined by the angular diversity of the flight path, and is located on a slant plane in the wave number space. The angle between the slant plane and the K_1, K_2-plane

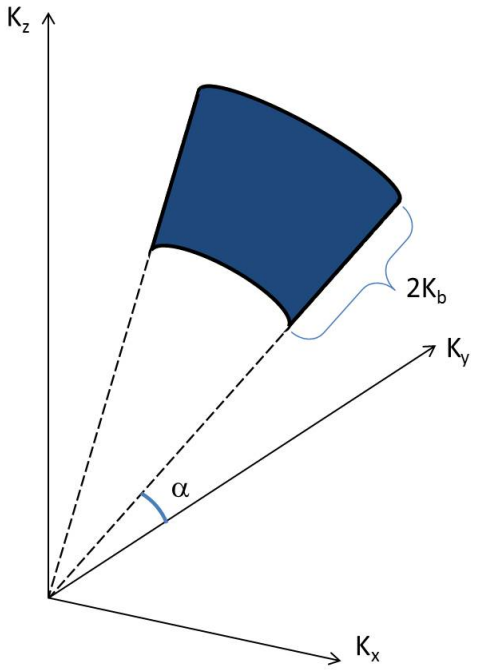

Figure III.2: Exampe of a 3-D SAR data collection annulus on the slant plane

will be equal to the angle of inclination of the between the ground plane and the radar antenna. In addition, the length of the annular region is determined by the $K_b = \frac{2\pi f_b}{c_0}$.

In this case, the goal is to produce a two dimensional image of the target scene. For this reason, it will be necessary project the collected data onto the ground plane. This can be accomplished by expanding (III.29) as follows

$$\begin{aligned} D(f,\phi) &= |P(f)|^2 \int_{-\infty}^{\infty}\int_{-\infty}^{\infty}\int_{-\infty}^{\infty} V(z_1,z_2,z_3) e^{i\frac{\widetilde{k}}{d}(rz_1\cos\phi + rz_2\sin\phi + hz_3)} dz_1 dz_2 dz_3 \\ &= |P(f)|^2 \int_{-\infty}^{\infty}\int_{-\infty}^{\infty}\left[\int_{-\infty}^{\infty} V(z_1,z_2,z_3) e^{i\frac{h\widetilde{k}}{d}z_3} dz_3\right] e^{i\frac{r\widetilde{k}}{d}(z_1\cos\phi + z_2\sin\phi)} dz_1 dz_2. \end{aligned} \tag{III.31}$$

It is now possible to define the modified reflectivity function $\widetilde{V}(\mathbf{y}) = \int_{\mathbb{R}} V(\mathbf{y}, z_3)\, e^{-i\frac{h\widetilde{k}}{d}z_3} dz_3$ where $\mathbf{y} = (z_1, z_2)^T$ and $\widetilde{k} = 2k$. Then, the expression in (III.29) is reduced to the two-dimensional Fourier transform of the modified reflectivity function $\widetilde{V}(\mathbf{y})$

$$\begin{aligned}\widetilde{D}(f,\phi) &= |P(f)|^2 \int_{\mathbb{R}^2} \widetilde{V}(\mathbf{y}) e^{-i\widetilde{k}\widehat{\boldsymbol{\mu}}(\phi)\cdot\mathbf{y}} d\mathbf{y} \\ &= |P(f)|^2 \mathscr{F}_{\mathbb{R}^2}\{\widetilde{V}\}(\mathbf{K}).\end{aligned} \tag{III.32}$$

Given a fixed angle ϕ, in the equation above, $\mathbf{K} = \widetilde{k}\widehat{\boldsymbol{\mu}}(\phi) = (\widetilde{k}\cos\phi, \widetilde{k}\sin\phi)^T$ corresponds to a set of lines through the origin. In the case of a single radar pulse at the angular position ϕ, the data function $\widetilde{D}(f,\phi)$ can be seen as an approximation of the Fourier transform of the reflectivity function $\widetilde{V}$ evaluated along a line corresponding to the fixed angle. The next chapter will illustrate how this idea can be used to solve the inversion problem to approximately recover the target reflectivity data in order to form a radar image. This will be accomplished through the application of the projection-slice theorem, which will be discussed in next chapter.

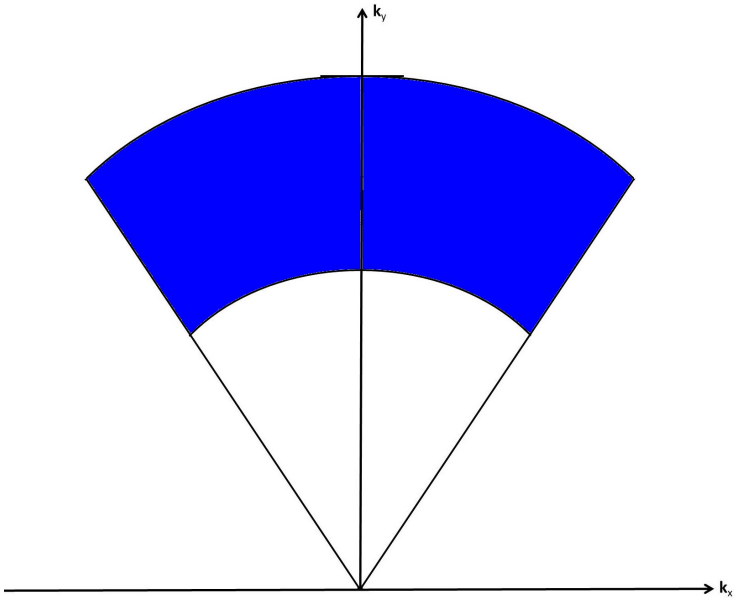

Figure III.3: 2-D SAR data collection annulus formed by the projection of the 3-D annulus on the ground plane

In Figure III.3, it can be seen that the data collection region corresponding to the two-dimensional imaging problem is an annular region, which is the projection of the data collection annulus in Figure III.2 onto the ground plane in the wave number domain. [17]

CHAPTER IV

CBP ALGORITHM AND SIMULATION RESULTS

In the previous chapter, an inversion method, which can be used to develop a CBP algorithm, was derived. This section demonstrates how this algorithm can be implemented for a circular SAR system. Also, a series of simulations based on this algorithm will be presented.

IV.1 Formulation Of The CBP Algorithm

In order to understand the mathematics of the CBP, it is first necessary to look at two important, but closely related, integral transforms. The first is the Radon transform, which is named after Johann Radon. The other is the X-ray transform. Both of these transforms are commonly found in inversion problems in a great variety of fields.

Conceptually, in two dimensions, the Radon transform is defined as the integral of a function f over the set of lines L in $\mathbb{R}^2$. There are a number ways in which the two dimensional Radon transform can be defined. These definitions only differ in the way that the lines are parameterized. Initially, the Radon transform will be defined only for the set of functions $f \in \mathscr{S}(\mathbb{R}^n)$, where $\mathscr{S}(\mathbb{R}^n)$ denotes the Swartz space over $\mathbb{R}^n$. However, more generally, the Radon transform can be defined for functions in $L^2(\mathbb{R}^n)$. The Radon transform is defined in terms of integration over the set of hyperplanes in $\mathbb{R}^n$, which are given by

$$H^n_{\widehat{\boldsymbol{\mu}},s} = \left\{ \mathbf{x} \in \mathbb{R}^n \mid \mathbf{x} \cdot \widehat{\boldsymbol{\mu}} = s \right\}.$$

In the above expression, $s \in \mathbb{R}$ and $\widehat{\boldsymbol{\mu}} \in S^{n-1}$, where S^{n-1} denotes the unit sphere in $\mathbb{R}^n$. In general, the output of the Radon transform of a function f on $\mathbb{R}^n$ is the function $\tilde{f}$ on the unit

cylinder $C^n = \mathbb{R} \times S^{n-1}$ in $\mathbb{R}^n$. Thus, the Radon Transform can be defined as follows

$$\tilde{f}(s, \widehat{\boldsymbol{\mu}}) = \mathcal{R}\{f\} = \int_{\mathbb{R}^n} f(\mathbf{x})\delta(s - \mathbf{x} \cdot \widehat{\boldsymbol{\mu}})d\mathbf{x}. \tag{IV.1}$$

In $\mathbb{R}^2$ let $\mathbf{x} = (x, y)$, and let the unit vector $\widehat{\boldsymbol{\mu}} \in S^1$ be denoted by $\widehat{\boldsymbol{\mu}}(\phi) = (\cos\phi, \sin\phi)^T$. Then for every $\mathbf{x} \in H^2_{\widehat{\boldsymbol{\mu}},\rho}$, it can be shown that there exists a constant $t \in \mathbb{R}$ such that $\mathbf{x} = s\widehat{\boldsymbol{\mu}} + t\widehat{\boldsymbol{\mu}}_\perp$, where $\widehat{\boldsymbol{\mu}}_\perp = (-\sin\phi, \cos\phi)^T$. Thus, the Radon transform is rewritten in terms of the following integral for all t.

$$\tilde{f}(s, \phi) = \int_{\mathbb{R}} f(s\cos\phi - t\sin\phi, s\sin\phi + t\cos\phi)dt. \tag{IV.2}$$

The definition of the Radon transform given above clearly denotes a set of projections over lines at a various angles. At this point it is appropriate to introduce the projection function p_ϕ, which is defined below.

Definition 1. *Let f be an integrable funtion on $\mathbb{R}^2$. Then, the projection of f at a fixed angle ϕ is given by $p_\phi(s) = \tilde{f}(s, \phi)$.*

In the case of higher dimensions, the X-ray transform is used to define the projection function instead of the Radon transform. This transform is generally used in three-dimensional radar applications. The X-ray transform differs from the Radon transform in that integration is always performed over the set of lines in $\mathbb{R}^n$. However, in two dimensions there is no distinction between these two transforms. The X-ray transform is commonly used in the formulation of the three dimensional backprojection algorithms .

There are a number of different reconstruction methods that can be developed based on the Radon and Ray transforms. One possibility would be to reconstruct the data contained in a single projection by directly inverting the Radon or X-ray transforms, as was originally suggested by Radon himself. However, most modern backprojection algorithms are based Fourier transform inversion instead. The next section will discuss how this can be accomplished.

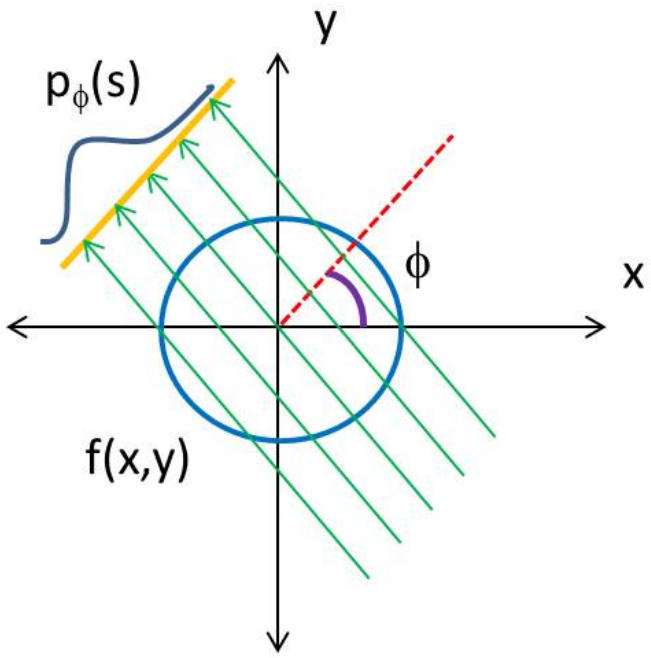

Figure IV.1: Projection Function

IV.2 Projection Slice Theorem

One of the most important developments, which allowed for the creation of the CBP algorithm, is the establishment of a mathematical relationship between the Radon transform and the Fourier transform. The relationship between these two transforms is given by the Projection-Slice Theorem (PST), which was first proved in the early 1950's. This theorem can be stated is stated below.

Theorem 1. *Given in integrable function f on $\mathbb{R}^2$ and a fixed angle ϕ*

$$\mathscr{F}_{\mathbb{R}^2}\{f\}(s\widehat{\boldsymbol{\mu}}(\phi)) = \mathscr{F}_{\mathbb{R}}\{p_\phi\}(s).$$

Intuitively, the PST indicates that the one-dimensional Fourier transform of the projection function p_ϕ is equal to the two-dimensional Fourier transform of $f(x, y)$ along a line at angle ϕ with the K_x-axis. This relationship is can be seen in Figure IV.2.

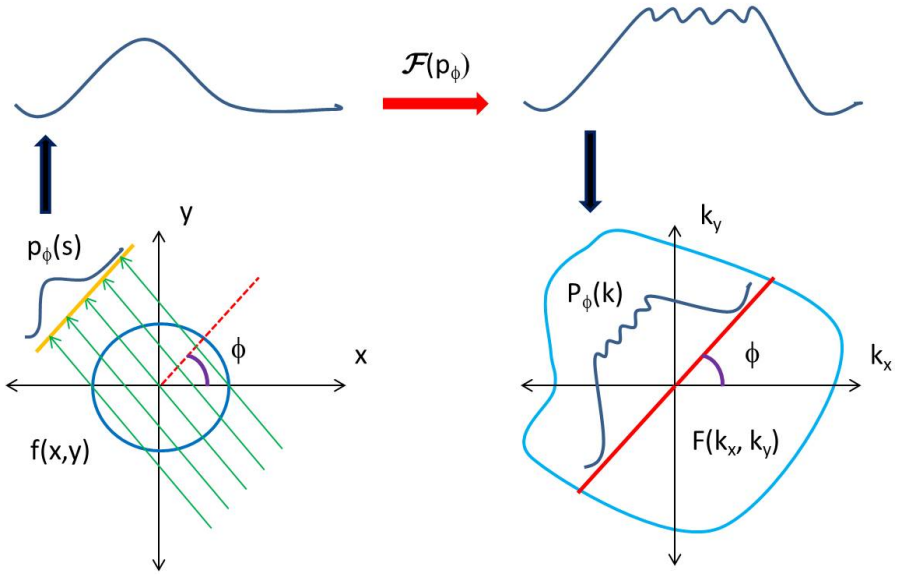

Figure IV.2: The Projection Slice Theorem

Then we will show that the radar image can be found through the inversion of Equation (III.32).

The pulse compressed version of the received signal $\tilde{D}$ is approximately equal to the Fourier transform of the ground reflectivity function $\widetilde{V}$. Now, in order to find a reconstruction algorithm for $\tilde{V}$, let E denote Fourier transform of $\widetilde{V}$ in $\mathbb{R}^2$ such that

$$E(\mathbf{K}) = \mathscr{F}\{\tilde{V}\} = \int_{\mathbb{R}^2} \tilde{V}(\mathbf{x}) e^{-i\mathbf{K}\cdot\mathbf{x}} d\mathbf{x}. \tag{IV.3}$$

The reconstructed image of the ground reflectivity function, which is denoted by I, can now be recovered by Fourier inversion of E such that $I(\mathbf{x}) = \mathscr{F}^{-1}(E)$. Next, the integral form of this expression can be written in terms of the polar coordinates $(\tilde{k}, \phi)$, where $\tilde{k} = -\dfrac{4\pi}{c_0} f$. In this case the equation for the recovered image becomes:

$$I(\mathbf{x}) = \frac{16\pi^2}{c_0^2} \int_0^\infty \int_0^{2\pi} E(f,\phi) e^{-i\frac{4\pi}{c_0} f(x\cos\phi + y\sin\phi)} f\, d\phi\, df. \tag{IV.4}$$

In accordance with the PST, given a fixed value of ϕ, $E(f,\phi) = P_\phi(f)$, where P_ϕ represents the Fourier transform of the projections of the ground reflectivity function $\tilde{V}(\mathbf{x})$. Let $\mathbf{x} = (\rho\cos\theta, \rho\sin\theta)^T$,

then the integral in equation (IV.4) becomes

$$I(\rho,\phi)=\frac{4\pi}{c_0^2}\int_0^{\infty}\int_0^{2\pi}P_\phi(f)e^{-i\frac{4\pi}{c_0}f\rho\cos(\theta-\phi)}fd\phi df. \tag{IV.5}$$

It is now possible to see that the name Convolution Backprojection comes from the fact that the inner integral is a circular convolution with the kernel function $L(f,\rho,\theta,\phi)=e^{-i\frac{4\pi}{c_0}f\rho\cos(\theta-\phi)}$. Generally, the CBP algorithm is not implemented in terms of equation (IV.4) in its current configuration. In this case, the inner integral would be performed through a fast circular convolution algorithm. That is to say that the inner integral would be computed by

$$\text{IFFT}\left\{\text{FFT}\left\{P_\phi(f)\right\}\text{FFT}\left\{L(f,\rho,\theta,\phi)\right\}\right\}.$$

The image could then be found by summing over the set of frequent samples, along with proper polar-to-rectangular interpolation. The problem with this algorithm is that it often requires that the kernel be sampled at a higher rate than the number of pulses. This means that an extra interpolation step must be added, which greatly reduces algorithmic efficiency. This step is referred to as the polar reformatting step, which is discussed by [1, 14, 15].

A more computationally efficient algorithm can be found by switching the order of integration in equation (IV.4) so that the frequency data is processed first. In this case, the image will be given by

$$I(\rho,\phi)=\int_0^{2\pi}Q(\rho,\phi)d\phi, \tag{IV.6}$$

where

$$Q(\rho,\theta,\phi)=\int_0^{\infty}P_\phi(f)e^{-i\frac{4\pi}{c_0}f\rho\cos(\theta-\phi)}fdf. \tag{IV.7}$$

One of the distinguishing characteristics of radar imaging is that data collected by radar systems are close approximations of the projection function in (IV.7). For this reason, $P_\phi(f)$ can be replaced

by the data function $\widetilde{D}(f,\phi)$, which was derived in the previous chapter. Then, $Q(\mathbf{x},\phi)$ reads as

$$Q(\mathbf{x},\phi) = \int_0^\infty \widetilde{D}(f,\phi) e^{-\frac{4\pi}{c_0} f(x_1\cos\phi + x_2\sin\phi)} f df. \tag{IV.8}$$

The integral in (IV.8) is generally implemented as an inverse Fourier transform over the frequency variable. Given discrete a set of radar data an IFFT is used in place of the inverse Fourier transform. The outer integral can then be implemented as a finite summation over the set angular data samples. [6, 11, 16]

IV.3 CBP Algorithm

The image will be recovered based on equation (IV.4), which can be rewritten as

$$I(x,y) = \int_{\phi_{\text{min}}}^{\phi_{\text{max}}} Q(x,y,\phi) d\phi. \tag{IV.9}$$

In general, radar imaging systems will only record data over a small set of angular samples. This is why the integral above has been restricted to an interval between $0 \leq \phi_{\text{min}} \leq \phi \leq \phi_{\text{max}} \leq 2\pi$.

In section V.3 it was stated that the projection function can be replaced by the modified data function $\widetilde{D}(f,\phi)$. The inner integral can now be defined as follows

$$Q(x,y,\phi) = \frac{4\pi}{c^2} \int_{f_{\text{min}}}^{f_{\text{max}}} \widetilde{D}(f,\phi) e^{-i\frac{4\pi}{c_0} f(x\cos\phi + y\sin\phi)} f df. \tag{IV.10}$$

In this integral, the minimum and maximum frequencies are defined in terms of the bandwidth and the carrier frequency such that $f_{\text{min}} = f_c - \frac{f_B}{2}$ and $f_{\text{max}} = f_c + \frac{f_B}{2}$.

The actual image formation will be performed in terms of a discreet set of samples such

$$f_j = f_{\text{min}} + (j-1)\Delta f \qquad \text{for } j = 1 \ldots K,$$

and

$$\phi_m = \phi_{\text{min}} + (m-1)\Delta\phi \qquad \text{for } m = 1 \ldots N.$$

At this point, a window function is often applied to the radar data in order to suppress the effect of sidelobes on the recovered data. In this case, a Hamming window, denoted by w_N, was chosen. Then, for fixed values of j and m, the data function will be given by

$$D(f_j, \phi_m) = (4\pi)^2 d^2 \overline{P(f_j)} e^{i\frac{4\pi}{c_0} f_j d} S(f_j, \phi_m) w_H(j). \tag{IV.11}$$

In the above equation, $d = \sqrt{r^2 + h^2}$ is the distance from the antenna to the target scene center. Then, for each projection, the data can be recovered in terms of a one-dimensional IFFT.

$$Q(x, y, m) = \frac{16\pi^2}{c^2} \text{IFFT}\{f_j D(j, m)\} \Phi(x, y, m), \tag{IV.12}$$

where

$$\Phi(x, y, m) = e^{-i\frac{4\pi}{c_0} f_{\min}(x\cos\phi + y\sin\phi)}.$$

The image is recovered in terms of a summation over the set of radar pulses

$$I(x, y) = \sum_{m=1}^{N} Q(x, y, m). \tag{IV.13}$$

IV.4 CBP Algorithm Summary

The processing of a received set of radar data can be divided into two stages. First the data is pre-processed. This results in a set of data that is equivalent to $D(j, m)$. The pre-processing phase for a set of received radar data is summarized as follows:

1. Multiply by $(4\pi)^2 d^2$ to compensate for geometric spreading.
2. Multiply by $e^{i\frac{4\pi}{c_0} f_j d}$ to compensate for the range offset.
3. Apply the pulse compression factor $\overline{P(f_j)}$.
4. Apply to the window function $w_H(j)$ to each pulse to suppress sidelobes.

Given this set of pre-processed data, the CPB algorithm can be used to recover the image of the target scene. The CBP algorithm is summarized as follows:

1. Set up a 2-D imaging grid.
2. For each pulse, prepare reference table, assigning each pixel a range value.
3. Apply a 1-D IFFT to the radar data for each pulse.
4. Interpolate the resulting range profile onto the image grid.
5. Multiply by the phase correction function Φ.
6. Sum over the radar pulses to form the final image.

IV.5 CBP Simulation Results

These simulations were performed in Matlab for a target scene depicting the outline of a vessel and a mobile car sitting on a landing strip. The target scene is made up of a series of point targets located at positions $\mathbf{y}_k$ on the target plane, where $k = 1 \dots M$. Hence, the reflectivity function was implemented using the formula

$$V(\mathbf{x}) = \sum_{k=1}^{\infty} \sigma_m \delta(\mathbf{x} - \mathbf{y}_k).$$

where σ_m is the reflectivity value for each point target. Then, the received signal is implemented using the formula

$$S(j,m) = \sum_{k=1}^{\infty} \sigma_k \frac{e^{-i\frac{4\pi}{c_0} f_j R(k,m)}}{(4\pi R(k,m))^2},$$

where

$$R(k,m) = |\mathbf{y}_m - \boldsymbol{\gamma}(\phi_m)|.$$

Both simulations were done with an angle inclination of $\alpha = 30^{\circ}$ with an antenna distance of 80 times the maximum target distance from the scene center. Also, the bandwidth of the transmitted signal is 400 kHz.

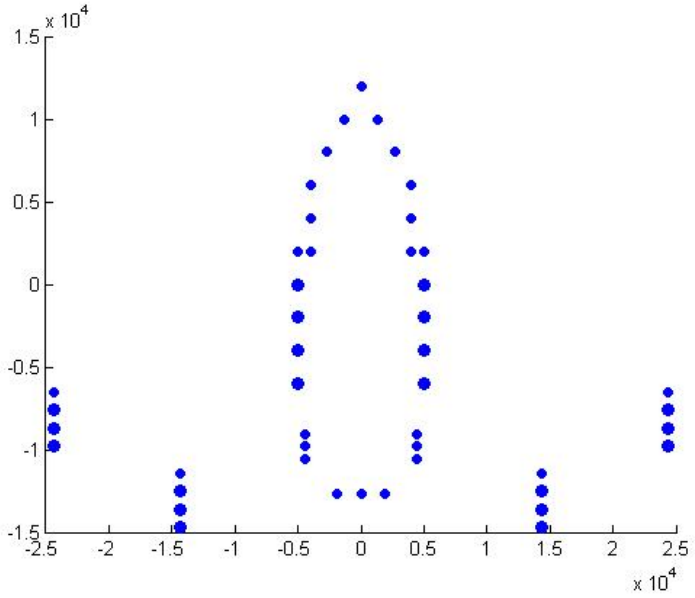

Target Scene.jpg

Figure IV.3: Actual Target Scene

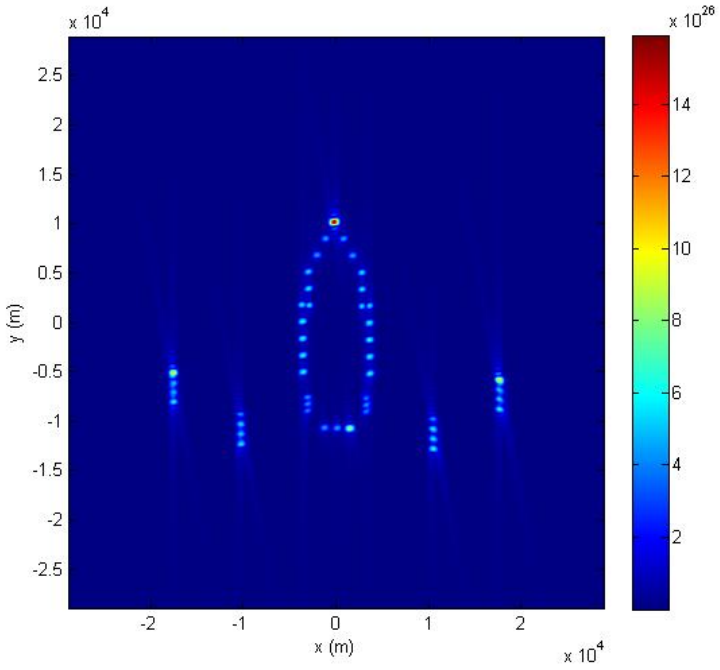

Image.jpg

Figure IV.4: CBP Image

Data Along a Single Projection.jpg

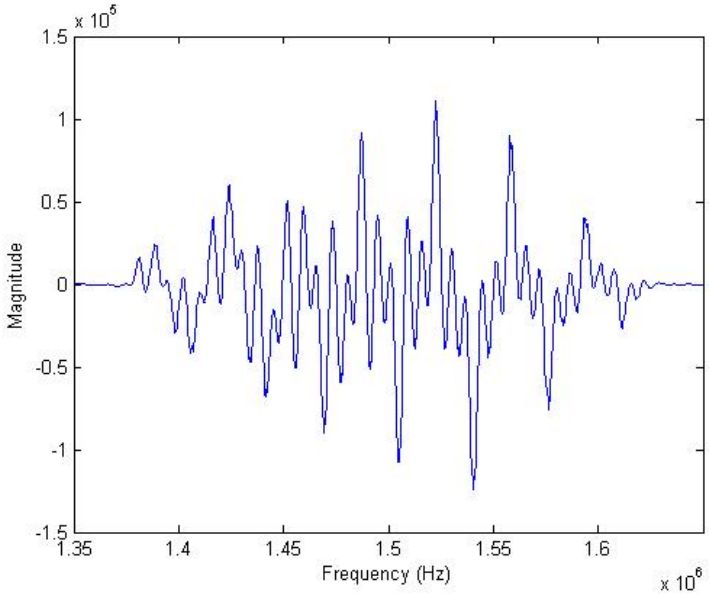

Figure IV.5: Collected Data Along a Single Projection(Boat)

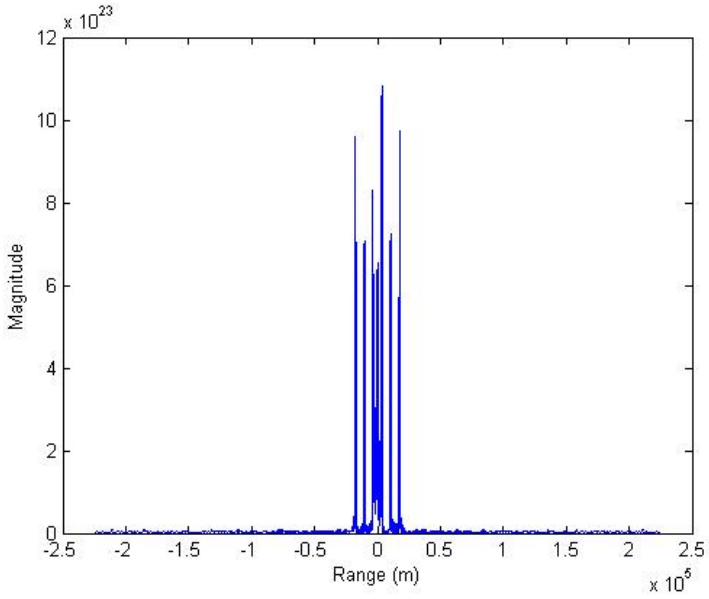

Range Profile afer IFFT.jpg

Figure IV.6: Resulting Range Profile afer IFFT(Boat)

profile interpolated to image grid.jpg

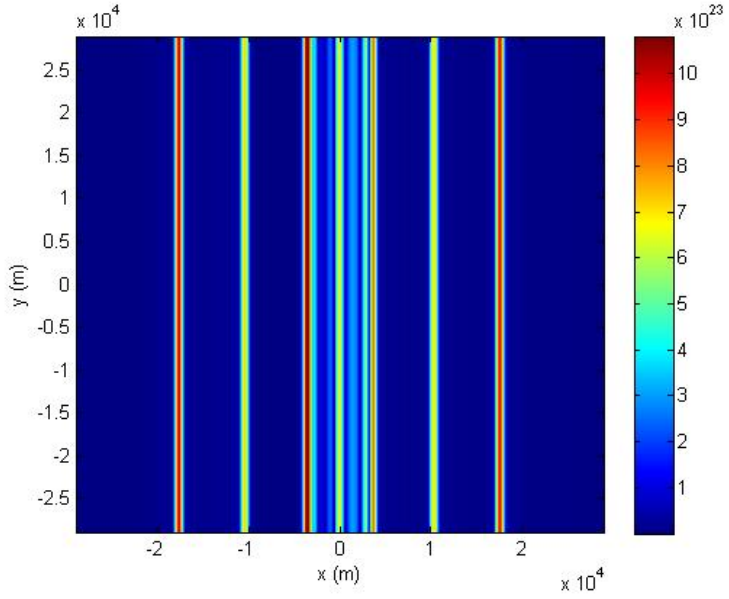

Figure IV.7: Range profile interpolated to image grid(Boat)

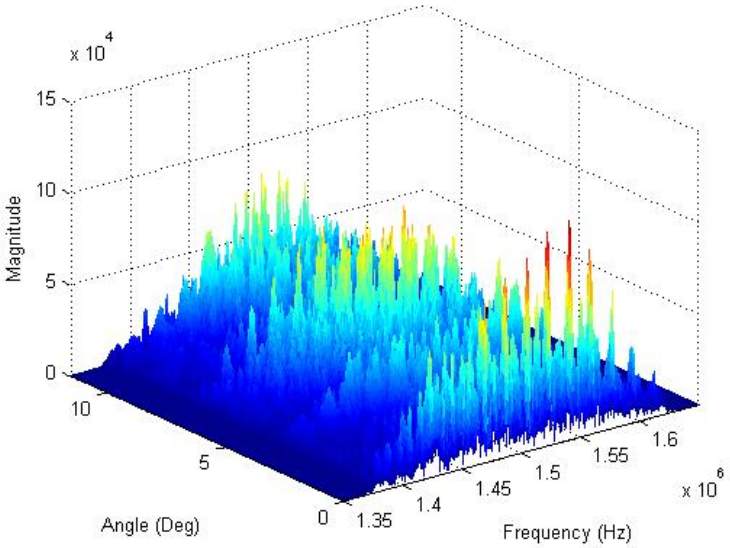

Data Set.jpg

Figure IV.8: Collected Data Set(Boat)

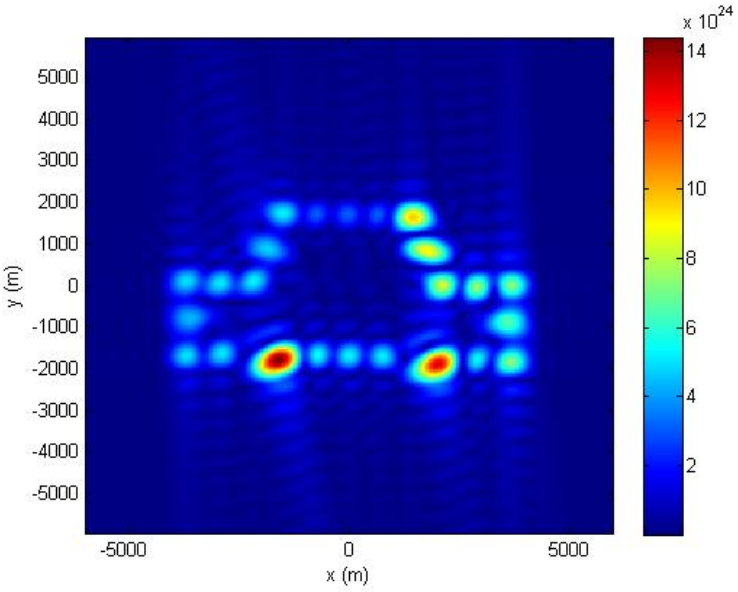

CBP Image.jpg

Figure IV.9: Car CBP Image

Resulting Range Profile afer IFFT.jpg

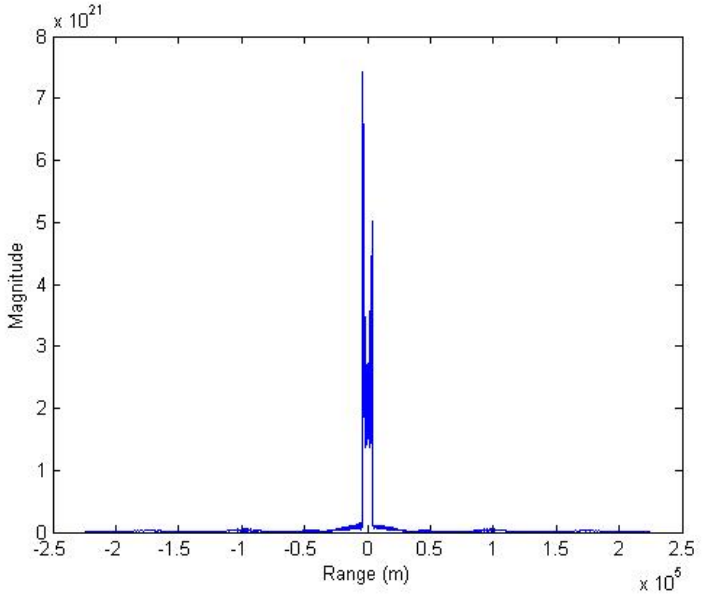

Figure IV.10: Car Resulting Range Profile afer IFFT

profile interpolated to image grid.jpg

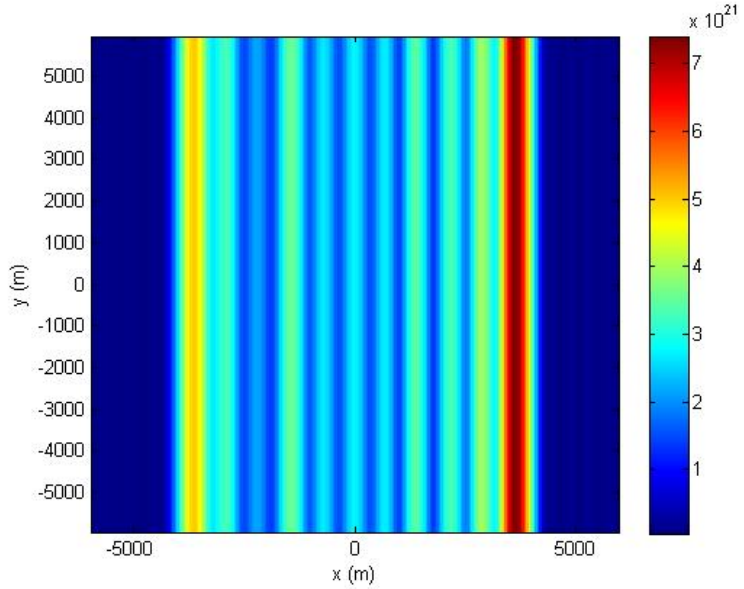

Figure IV.11: Range profile interpolated to image grid II

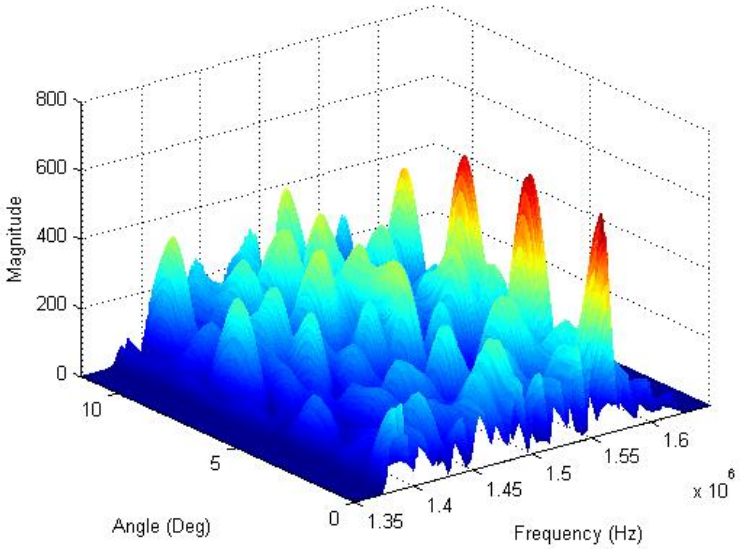

Data Set.jpg

Figure IV.12: Collected Data Set II

CHAPTER V

CONCLUSION

In this thesis, backprojection algorithms are used because they produce high quality images. However, this image quality comes at the expense of poor time efficiency. This method of high resolution image formation can be easily expanded to form images for spotlight-mode SAR systems. The CBP was formulated in terms of a wave model, which is based on Maxwell's equations. It was shown that the received radar data is approximately inverted using the inverse Fourier fransform. The projection-slice theorem was then used to show how the image could be accurately recovered from the set of received radar data. Finally, the ability of the CBP algorithm to produce high resolution images was demonstrated through a set of Matlab simulations.

REFERENCES

[1] Antoni Broquetas, Josep Palau, Luis Jofre, and Angel Cardama. Spherical wave near-field imaging and radar cross-section measurement. *Antennas and Propagation, IEEE Transactions on*, 46(5):730–735, 1998.

[2] Walter G Carrara, Ron S Goodman, Ronald M Majewski, et al. *Spotlight synthetic aperture radar: signal processing algorithms*. Artech House Boston, 1995.

[3] Margaret Cheney and Brett Borden. *Fundamentals of radar imaging*, volume 79. Siam, 2009.

[4] Ian G Cumming and Frank H Wong. *Digital signal processing of synthetic aperture radar data: algorithms and implementation*. Artech House, 2004.

[5] John C Curlander and Robert N McDonough. *Synthetic aperture radar*, volume 199. Wiley New York, 1991.

[6] Joaquim Fortuny and Alois J Sieber. Fast algorithm for a near-field synthetic aperture radar processor. *Antennas and Propagation, IEEE Transactions on*, 42(10):1458–1460, 1994.

[7] Guillermo Garza and Zhijun Qiao. Resolution analysis of bistatic sar. In *SPIE Defense, Security, and Sensing*, pages 80211V–80211V. International Society for Optics and Photonics, 2011.

[8] Achim Hein. *Processing of SAR data: fundamentals, signal processing, interferometry*. Springer, 2004.

[9] Charles V Jakowatz, Daniel E Wahl, Paul H Eichel, Dennis C Ghiglia, and Paul A Thompson. *Spotlight-mode synthetic aperture radar: a signal processing approach*, volume 101. Kluwer Academic Publishers Boston, USA:, 1996.

[10] Jaime X Lopez and Zhijun Qiao. Filtered back projection inversion of turntable isar data. In *Proc. SPIE*, volume 8051, page 805109, 2011.

[11] Jaime Xavier Lopez. *Inverse synthetic aperture radar imaging theory and applications*. THE UNIVERSITY OF TEXAS-PAN AMERICAN, 2011.

[12] Soumekh Mehrdad. Synthetic aperture radar signal processing with matlab algorithms. *A Wily Interscience Publication*, 1999.

[13] David C Munson Jr, James D O'Brien, and W Jenkins. A tomographic formulation of spotlight-mode synthetic aperture radar. *Proceedings of the IEEE*, 71(8):917–925, 1983.

[14] K Nicholson and C Wang. Improved near-field radar cross-section measurement technique. *IEEE Antennas and Wireless Propagation Letters*, 8:1103–1106, 2009.

[15] Jerry L Prince. A convolution backprojection formula for three-dimensional vector tomography. In *Image Processing, 1994. Proceedings. ICIP-94., IEEE International Conference*, volume 2, pages 820–824. IEEE, 1994.

[16] Timothy P Ray, Jaime X Lopez, and Zhijun Qiao. Principles of 3d turntable radar imaging. In *Radar Conference (RADAR)*, pages 0758–0763. IEEE, 2012.

[17] Bing Sun, Zhijun Qiao, and Jie Chen. Outer circular synthetic apeture radar imaging based on maxwell's equations. *Journal of Applied Remote Sensing*, 6(1):063547–1, 2012.

[18] Jack L Walker. Range-doppler imaging of rotating objects. *Aerospace and Electronic Systems, IEEE Transactions on*, (1):23–52, 1980.

BIOGRAPHICAL SKETCH

Qitong Li was born in Dalian, Liaoning in 1988. In 2012, he graduated with honors with a B.Sc. in Mathematics from the Shanghai University. Later he continued his education in University of Texas-Pan American by earning his M.Sc. in Mathematical Sciences in 2014.